Journal of ELECTRONIC MATERIALS, Vol. 45, No. 8, 2016
DOI: 10.1007/s11664-016-4600-8

Nitrogen Dioxide-Sensing Properties at Room Temperature of Metal Oxide-Modified Graphene Composite via One-Step Hydrothermal Method

DONGZHI ZHANG,[1,2] JINGJING LIU,[1] and BOKAI XIA[1]

1.—College of Information and Control Engineering, China University of Petroleum (East China), Qingdao 266580, People's Republic of China. 2.—e-mail: dzzhang@upc.edu.cn

A metal oxide/graphene composite film-based sensor toward room-temperature detection of ppm-level nitrogen dioxide (NO_2) gas has been demonstrated. The sensor prototype was constructed on a PCB substrate with microelectrodes, and a tin oxide-reduced graphene oxide (SnO_2-rGO) composite as sensing film was prepared by one-step hydrothermal synthesis of tin tetrachloride pentahydrate solution in the presence of graphene oxide (GO). The SnO_2–rGO hybrid composite was examined by scanning electron microscope and x-ray diffraction (XRD). The gas sensing properties of the SnO_2-rGO composite were investigated at room temperature by exposing it to a wide concentration ranging from 1 ppm to 2000 ppm toward NO_2 gas. The experiment results showed that the sensor exhibited a high response, superior selectivity, good repeatability, rapid response/recovery characteristics and low detection limit of 1 ppm, which exceeded that of a pure rGO sensor. The gas sensing mechanisms of the proposed sensor toward NO_2 were possibly attributed to the nano-hybrid structures and *n*–*p* heterojunctions created at the interface of the SnO_2 nanocrystals and rGO nanosheets.

Key words: Hydrothermal synthesis, reduced graphene oxide, composite film, nitrogen dioxide sensor, room temperature

INTRODUCTION

Nitrogen dioxide (NO_2) is one of major compounds of vehicle exhausts, as well as the main emission from thermal power plants and chemical production processes.[1–4] Furthermore, NO_2 gas is not only an atmospheric pollutant harmful to environment but also a toxic gas resulting in some serious diseases of human beings. Because of its noxiousness for health and the environment, extremely precise quantitative detection of NO_2 gas has attracted considerable attention. Until now, a number of methods have been devoted to NO_2 detection, such as spectrophotometry,[5] photo-acoustic,[6] chemiresistive,[7] potentiometric,[8] amperometric,[9] optical fiber,[10] surface acoustic wave (SAW),[11] and quartz crystal microbalance (QCM).[12] However, these methods have their own shortcomings, such as time consuming, not suitable for portable use, and requiring expensive equipment, limiting their wide application.[13] Recently, considerable attention has been attracted to metal-oxide semiconducting (MOS) material-based sensors for NO_2 detection, such as indium-tin-oxide,[14] tungsten trioxide (WO_3),[15] tin oxide (SnO_2),[16] and zinc oxide (ZnO),[17] which are widely used. These sensors have exhibited great potential in terms of sensitivity, small size, and fast response and recovery times, but mostly have a dependence on high operating temperatures, resulting in high power consumption and difficulty in integration. Therefore, exploring a novel sensing material and method toward NO_2 detection at room temperature is highly desired.

Graphene is an emerging two-dimensional material that possesses extraordinary electrical and mechanical properties that promise a new generation

(Received December 9, 2015; accepted April 28, 2016; published online May 10, 2016)

of innovative devices.[18–20] Various graphene-based devices have been proposed and have demonstrated a huge opportunity for practical applications.[21,22] Although great potential has reported for various gas species on graphene, special problems such as long response time and narrow detection range have restricted its commercialization. Notably, graphene-based metal oxide hybrid composites are emerging as a class of candidate materials to construct high-performance gas sensors. Deng et al. fabricated a NO_2 gas sensor using reduced graphene oxide (rGO)-conjugated Cu_2O nanowire mesocrystals as sensing materials,[23] and Srivastava et al. exploited graphene–WO_3 nanocomposite for a faster response in NO_2 sensing.[24] Jiang et al. successfully synthesized paper-like Fe_2O_3/graphene nanosheets as sensing materials to detect H_2S gas.[25] Singh et al. have reported that ZnO-decorated luminescent graphene exhibited a good response toward CO, NH_3 and NO_2 at room temperature.[26] Neri et al. reported sol–gel-synthesized SnO_2/rGO nanocomposites on alumina substrates, and their sensing characteristics toward 8 ppm NO_2 were investigated at an operating temperature around 200°C.[27] Room-temperature-operated gas sensors with the advantages of low power consumption and easy integration are highly desirable.

This paper demonstrates a ppm-level NO_2 gas sensor based on a tin oxide-reduced graphene oxide (SnO_2-rGO) hybrid composite. The sensor prototype was fabricated on a PCB substrate with microelectrodes. The nanostructural, morphological and compositional properties of the SnO_2–rGO hybrid composite was inspected by SEM and XRD. The sensing properties of the sensor were investigated at room temperature toward NO_2 gas over a wide concentration. The sensing performance such as sensitivity, response/recovery times, repeatability and stability have been demonstrated. Furthermore, the possible sensing mechanism of SnO_2–rGO hybrid film toward NO_2 gas has been discussed.

EXPERIMENTAL

Chemical Reagents and Materials

Tin tetrachloride pentahydrate ($SnCl_4{\cdot}5H_2O$) (≥99%) was obtained from Shanghai Hansi Chemical Industry (Shanghai, China), and the commercial available high-purity GO nanosheets (>99%) were supplied by Chengdu Organic Chemicals (Chengdu, China). All the above chemicals were used as received without further treatment.

Sensor Fabrication

The sensor was fabricated on a low-cost PCB substrate with a pair of rectangular-ambulatory-plane interdigital electrodes (RAP-IDEs). Figure 1 shows the optical image of the sensor structure on the substrate. The sensing film of the SnO_2–rGO hybrid composite was prepared through hydrothermal treatment of $SnCl_4$ solution in the presence of GO. First, $SnCl_4{\cdot}5H_2O$ and GO were added to 20 mL of deionized (DI) water by ultrasonic treatment for 10 min and stirring for 1 h, followed by transferring the above solution into a stainless steel autoclave and heated at 180°C for 12 h. GO was converted into conductive rGO under hydrothermal reduction. The as-prepared products were obtained via centrifugation at 3000 rpm for 10 min, and subsequently washed several times with DI water to remove excess chloride ion. Finally, the resulting SnO_2-rGO dispersion was drop-coated onto the substrate, followed by vacuum-drying in an oven at 50°C for 2 h. For the purpose of making comparisons, the rGO film sensor was prepared for subsequent use by the above method but without the addition of $SnCl_4{\cdot}5H_2O$.

Experimental Setup

The experiment was performed under specific conditions (30% RH, room temperature of 25°C). The gas-sensing properties of the sensor were investigated by exposing the sample to various concentrations of NO_2 gas, ranging from 1 ppm to 2000 ppm. The desired gas concentration was obtained by injecting the required quantity of NO_2 gas into a sealed chamber using a syringe. The sensor response in resistance was recorded by using a data logger (Agilent 34970A, USA), which was connected to a computer via a RS-232 interface. The figure-of-merit used to characterize the sensor performance was the normalized response (S), determined by $S = (R_a - R_g)/R_a \times 100\%$, where R_g and R_a are the electrical resistance of the sensor in the given concentration of NO_2 gas and air, respectively.

RESULTS AND DISCUSSIONS

Sample Characterization

The surface micromorphology of the rGO film and SnO_2–rGO hybrid composite were characterized by field emission scanning electron microscopy

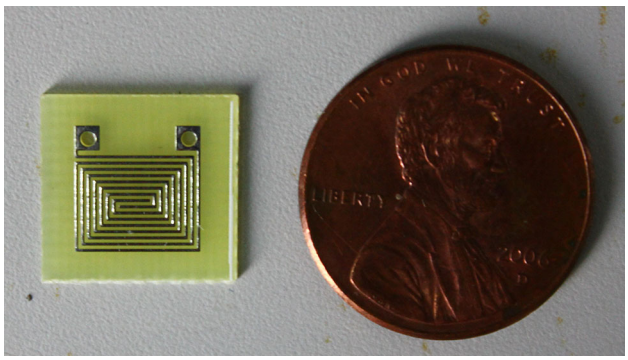

Fig. 1. Optical image of the sensor structure on a PCB substrate.

(FESEM; Hitachi S-4800). Furthermore, the microstructures of rGO film and SnO_2–rGO hybrid composite were performed with an x-ray diffractometer (Rigaku D/Max 2500PC).

Figure 2 shows the observed SEM images of as-prepared rGO film and the SnO_2–rGO hybrid composite. The SEM image of rGO in Fig. 2a indicates that the rGO film has wrinkles which overlap at the edges, and exhibits randomly aggregated rGO sheets. The result in Fig. 2b shows that SnO_2 nanocrystals are attached on the surface of the rGO sheets, in which the presence of SnO_2 nanocrystals reveals that hydrothermal treatment of GO and $SnCl_4$ solution is an effective method for synthesizing the SnO_2–rGO hybrid composite.

The XRD characterization for rGO, SnO_2 and SnO_2-rGO is illustrated in Fig. 3. The XRD analysis was carried out by using Cu Kα (λ = 1.5418 Å) radiation, with a scanning range of the diffraction angle (2θ) of 10°–80°. The XRD pattern of the rGO in Fig. 3a shows a prominent peak at the 2θ angle of 24.7°, and the interlayer distance d can be determined as 3.60 Å according to the Bragg formula, $\lambda = 2d\sin(\theta)$. The XRD pattern of the SnO_2 nanocrystals in Fig. 3b exhibits several strong scatting peaks attributed to the different corresponding planes of the nanocrystals. Figure 3c shows the XRD spectrum of the SnO_2–rGO hybrid in which the broad peak for rGO is not obvious, probably due to the rGO being wrapped by SnO_2 nanoparticles during hydrothermal synthesis.

NO_2-Sensing Properties

Figure 4 shows the response transients of the SnO_2–rGO hybrid composite sensor exposed to different concentrations of NO_2 gas. The sensing behavior of the sensor was investigated at room temperature by exposing it to a wide concentration range from 1 ppm to 2000 ppm NO_2 gas. It is obvious that the responses of the sensor changed rapidly on being exposed to air and to NO_2. When the sensor was exposed to different concentrations of 1 ppm, 5 ppm, 10 ppm, 50 ppm, 100 ppm, 500 ppm, 1000 ppm and 2000 ppm NO_2 gas, the corresponding response was almost up to 1.91%, 2.53%, 3.14%, 3.45%, 5.11%, 11.24%, 22.87% and 28.15%, respectively. It was found that the sensor yielded a low detection limit of 1 ppm at room temperature.

Figure 5 demonstrates the repeatability and stability of the SnO_2–rGO hybrid composite sensor under four different concentrations of NO_2 gas at room temperature. The repeatability characteristic was measured for five exposure/recovery cycles repeatedly to 1 ppm, 10 ppm, 100 ppm and 1000 ppm, respectively. The excellent response/recovery behavior and acceptable repeatability of the presented sensor toward NO_2 sensing are shown.

In order to further investigate the response and recovery times of the SnO_2-rGO film sensor toward different concentrations of NO_2 gas, Fig. 6 shows the time-dependent response of the sensor to 1 ppm,

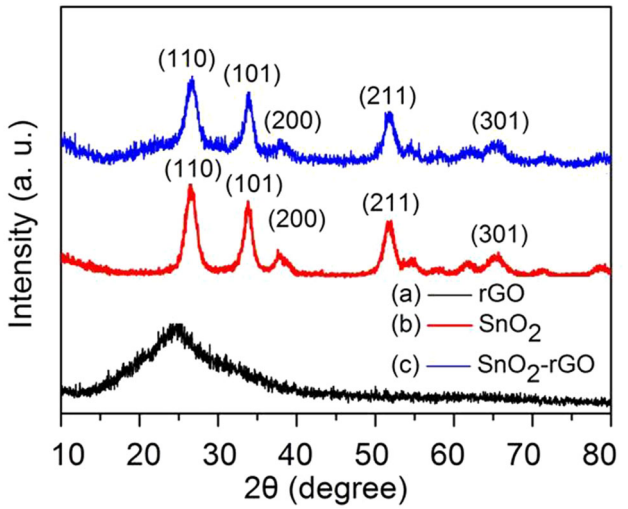

Fig. 3. XRD pattern for (a) rGO, (b) SnO_2, and (c) SnO_2–rGO hybrid composite (Color figure online).

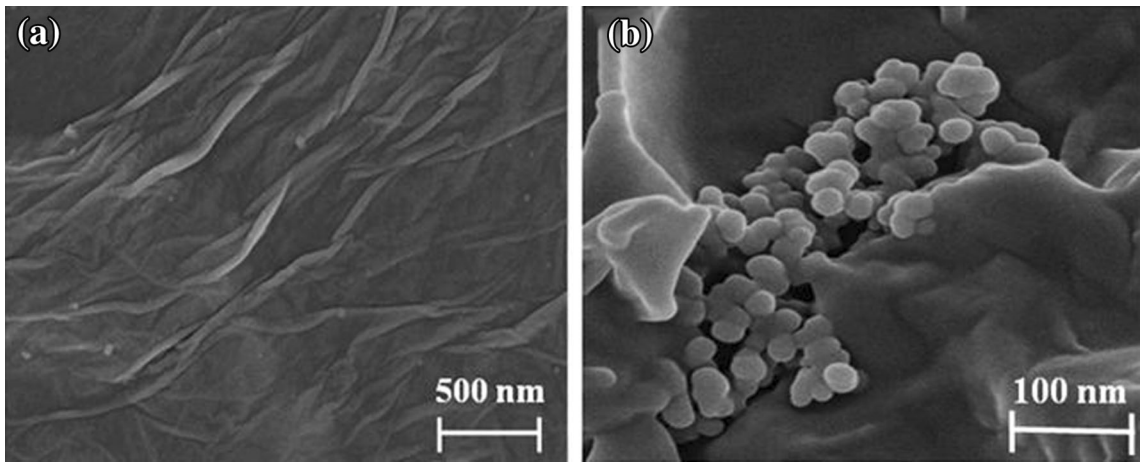

Fig. 2. SEM characterization of (a) rGO film and (b) SnO_2–rGO hybrid film.

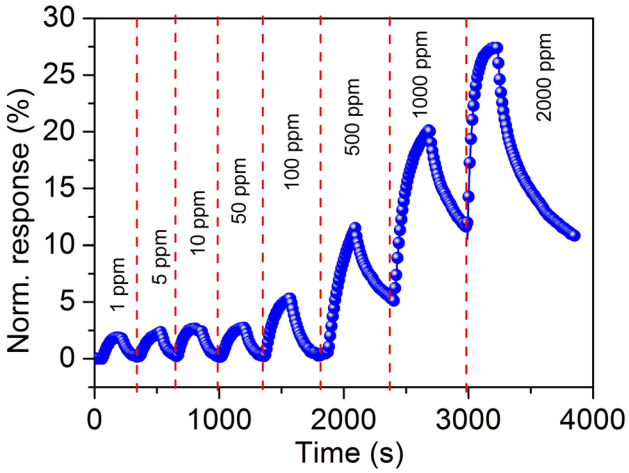

Fig. 4. Response transients of the SnO_2–rGO hybrid composite sensor to different concentrations of NO_2 gas.

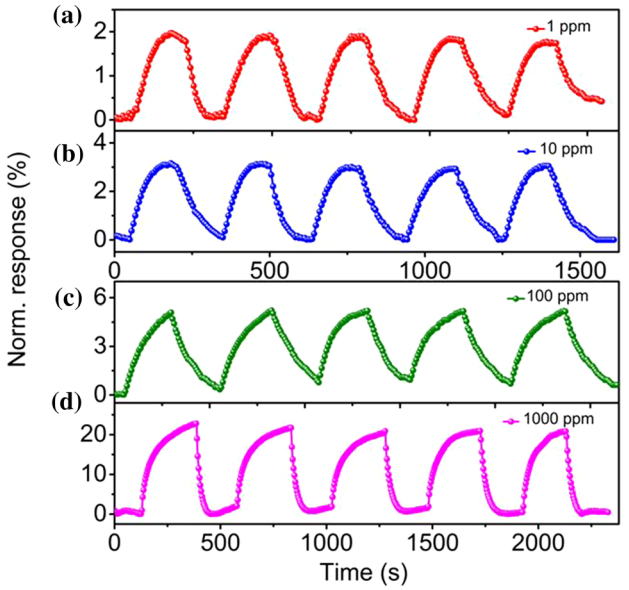

Fig. 5. Repeatability of the SnO_2–rGO hybrid composite sensor upon exposure to (a) 1 ppm, (b)10 ppm, (c) 100 ppm, and (d) 1000 ppm of NO_2 gas, respectively.

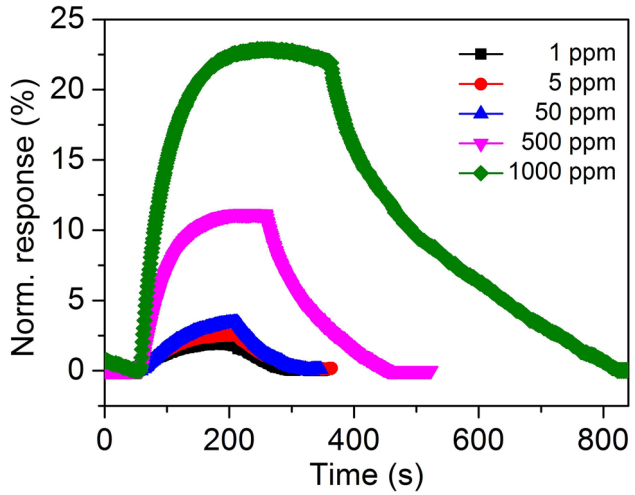

Fig. 6. Time-dependent response/recovery curves of the SnO_2–rGO hybrid composite sensor exposed to various concentrations of NO_2 gas (Color figure online).

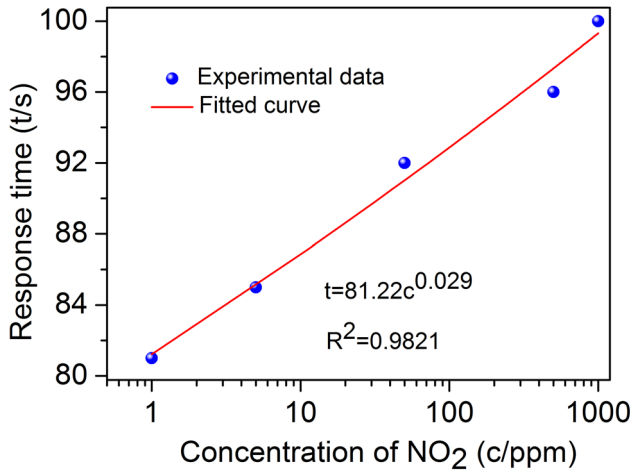

Fig. 7. Relationship of response time with gas concentration of NO_2 for the sensor (Color figure online).

5 ppm, 50 ppm, 500 ppm, 1000 ppm NO_2 gas and recovery in air. The response time of the presented sensor is about 81–100 s toward different concentrations. The relationship of the response time to the concentration of NO_2 was further investigated as shown in Fig. 7. The fitting equation of response time for the SnO_2–rGO hybrid film sensor and NO_2 concentration can be represented as $t = 81.22c^{0.029}$, and the fitting correlation coefficient, R^2, is 0.9821.

Figure 8 shows the normalized response of the SnO_2–rGO hybrid film sensor as a function of NO_2 gas concentration. The fitting equation for the normalized response Y as a function of NO_2 concentration X can be represented as $Y = 0.2348e^{\lg X/0.6911} + 1.4956$, and the fitting correlation coefficient, R^2, is 0.9656. It is obvious that the sensor response is increased with the rising concentration over a wide detection range of 1–2000 ppm toward NO_2 gas.

Figure 9 illustrates the performance comparison between the SnO_2–rGO hybrid composite and the pure rGO film sensor toward NO_2. The gas sensing test was performed by exposing the two sensors to 50 ppm, 500 ppm and 1000 ppm of NO_2 at room temperature. The comparison results indicated that the SnO_2–rGO hybrid composite sensor yielded several-fold higher responses than that of the pure rGO film sensor. Moreover, the response and recovery times of the SnO_2–rGO hybrid composite sensor are much shorter than for the rGO film sensor. Therefore, the SnO_2–rGO hybrid composite sensor is superior to the pure rGO film sensor in NO_2 gas sensing. Furthermore, the selectivity characteristic

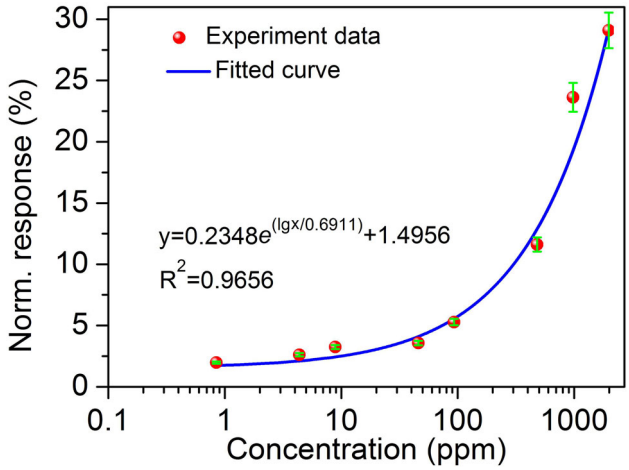

Fig. 8. Normalized response of the SnO_2-rGO film sensor as a function of NO_2 concentrations of gas (Color figure online).

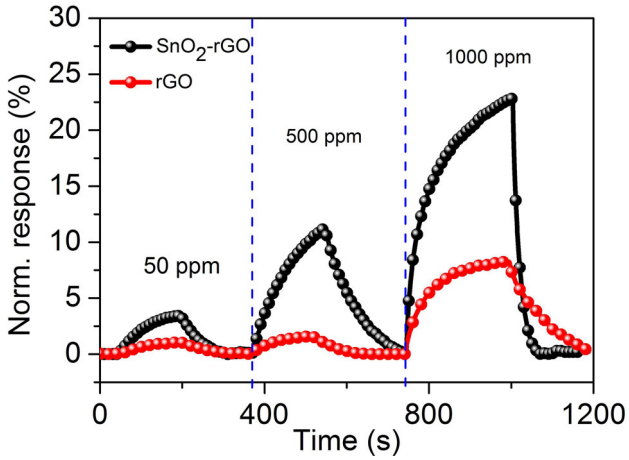

Fig. 9. Performance comparison between the SnO_2–rGO hybrid composite sensor and the pure rGO film sensor toward NO_2 gas (Color figure online).

of the SnO_2–rGO hybrid composite sensor toward NO_2 gas was also investigated. Figure 10 illustrates the measured selectivity of the sensor to 100 ppm of various gas species at room temperature, including NO_2, methane, hydrogen, carbon dioxide, sulfur dioxide and acetone. It is clearly observed that the sensor response to NO_2 gas was much higher than those of other tested vapors at the same concentrations.

Gas-Sensing Mechanism

The above-mentioned experimental results demonstrate that the SnO_2–rGO hybrid composite sensor has a good sensing performance toward NO_2 at room temperature, including higher response, shorter response and recovery times, and better repeatability and stability. The enhancement of the gas sensing performances of the SnO_2-rGO-based sensor can be attributed to the co-operative action of the SnO_2 nanocrystals and rGO nanosheets.[28–30] The

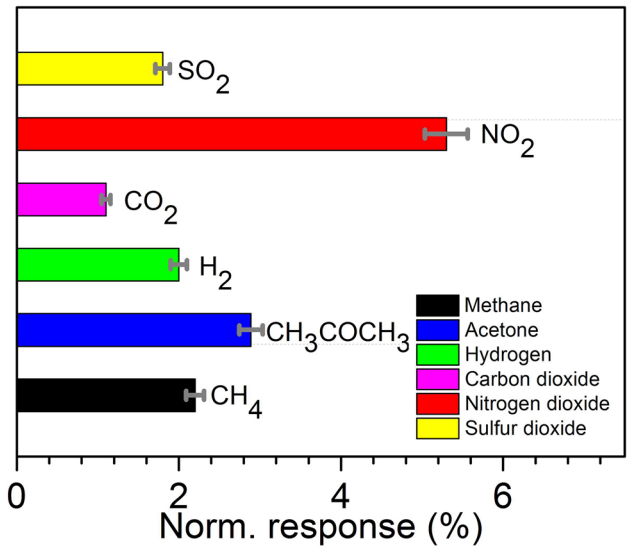

Fig. 10. Response of the SnO_2–rGO hybrid composite sensor toward 100 ppm of NO_2, CH_4, H_2, CO_2, SO_2 and CH_3COCH_3 at room temperature (Color figure online).

introduction of SnO_2 nanoparticles plays a role in preventing the aggregation of rGO sheets and forming a nano-hybrid structure with much higher surface accessibility, which greatly facilitates the adsorption and diffusion of the NO_2 gas molecules. The decoration of the SnO_2 nanocrystals on the rGO sheets leads to more active sites for the adsorption of gas molecules, and, thus, a higher response for the sensor was obtained in comparison with that of pure rGO. In addition, rGO is a highly conductive sp^2 carbon atom film, serving as a paddle to promote the free electrons transfer in the metal oxide nanoparticles, thus leading to a better response/recovery characteristic.

The gas-sensing mechanism associated with the heterojunction formed at the interface of rGO and SnO_2 is supposed to make another important contribution. SnO_2 is an *n*-type semiconducting material with a wide bandgap of 3.6 eV, and the incorporation of *p*-type rGO nanosheets on the SnO_2 nanocrystals creates *p*–*n* heterojunctions at the interface of SnO_2 and graphene, as reported in Refs. 31, 32, and 33. The SnO_2–rGO junction and the action mechanism for the sensor are shown in Fig. 11. The oxygen molecules in air are absorbed on the conduction band of SnO_2, and these surface-adsorbed molecules are ionized to oxygen ions with a single negative charge through capturing free electrons from the surface of the SnO_2.[34–36] The reaction can be summarized as shown in Eqs. 1 and 2. The space charge region (the depletion layer) is created by the oxygen ions on the SnO_2 surface, making the sensor be in a high resistance state in air. Once the sensor upon exposure toward NO_2 gas, the adsorption of NO_2 gas molecules becomes involved in the oxidation reaction with surface oxygen ions adsorbed on the surface, which is described as shown in Eqs. 3 and 4. The differences

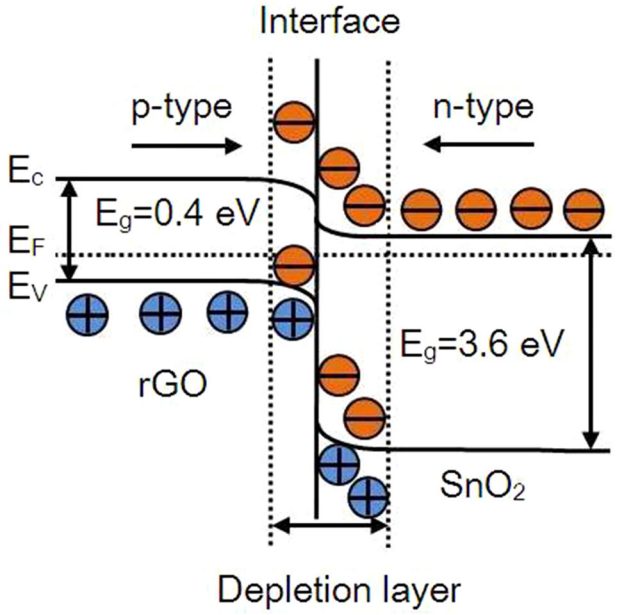

Fig. 11. SnO_2-rGO junction and action mechanism for the sensor.

in the bandgap and Fermi level between rGO and SnO_2 are modified through band bending in the depletion layer when adsorbing or desorbing targeted gas molecules. Such a reaction causes a release of electrons captured in the ionized oxygen species which return into the SnO_2 conduction band, thus increasing the concentration of free electrons and decreasing the measured sensor resistance.

$$O_2(\text{gas}) \rightarrow O_2(\text{ads}) \quad (1)$$

$$O_2(\text{ads}) + e^- \rightarrow O_2^-(\text{ads}) \quad (2)$$

$$NO_2 + e^- \rightarrow NO_2^- \quad (3)$$

$$2NO_2^- + O_2^- \rightarrow 2NO^- + 2O_2 + e^- \quad (4)$$

CONCLUSIONS

We prepared a SnO_2–rGO hybrid composite by one-step facile hydrothermal synthesis and constructed a ppm-level NO_2 gas sensor on a PCB substrate by a low-cost fabrication method. The film of the SnO_2–rGO hybrid composite was inspected by SEM and XRD. Its sensing behaviors toward NO_2 were investigated by exposing the sensor to NO_2 gas over wide concentrations ranging from 1 ppm to 2000 ppm. The sensing performance such as sensitivity, response/recovery times, repeatability and stability were demonstrated. The possible mechanism of NO_2 gas sensing for the SnO_2–rGO hybrid composite sensor was attributed to the *p*–*n* heterojunction formed at the interface of the SnO_2/graphene composite or the electron transfer between the surface-absorbed oxygen species and NO_2 gas molecules.

ACKNOWLEDGEMENTS

We acknowledge the funding support from the National Natural Science Foundation of China (No. 51407200), the Science and Technology Development Plan Project of Shandong Province of China (No. 2014GSF117035), the Fundamental Research Funds for the Central Universities of China (Grant No. 15CX05041A), and the Science and Technology Project of Huangdao Zone, Qingdao, China (No. 2014-1-51).

REFERENCES

1. C. Zhang, J. Wang, M.G. Olivier, and M. Debliquy, *Sens. Actuators B* 209, 69 (2015).
2. P. Jasinski, A. Strzelczyk, B.A. Chachulski, M. Gazda, and G. Jasinski, *Sens. Actuators B* 189, 141 (2013).
3. A. Sen, K.A. Kupcho, B.A. Grinwald, H.J. Vantreeck, and B.R. Acharya, *Sens. Actuators B* 178, 222 (2013).
4. T. Xie, G.Z. Xie, Y. Zhou, J.L. Huang, M. Wu, Y.D. Jiang, and H.L. Tai, *Chem. Phys. Lett.* 614, 275 (2014).
5. A. Aydm, Ö. Ercan, and S. Tascioglu, *Talanta* 66, 1181 (2005).
6. M.A. Gondal and M.A. Dastageer, *J. Environ. Sci. Health A* 45, 1406 (2010).
7. Y.X. Zhang, J.J. Kim, D. Chen, H.L. Tuller, and G.C. Rutledge, *Adv. Funct. Mater.* 24, 4005 (2014).
8. Y. Chen and J.Z. Xiao, *Sens. Actuators B* 192, 730 (2014).
9. M. Nádherná, F. Opekar, J. Reiter, and K. Štulík, *Sens. Actuators B* 161, 811 (2012).
10. C. Tyszkiewicz, P. Karasinski, and R. Rogozinski, *Acta Phys. Pol. A* 122, 915 (2012).
11. S.H. Wang, S.H. Kuo, and C.Y. Shen, *Sens. Actuators B* 156, 668 (2011).
12. N.V. Quy, V.A. Minh, N.V. Luan, V.N. Hung, and N.V. Hieu, *Sens. Actuators B* 153, 188 (2011).
13. S. Liu, B. Yu, H. Zhang, T. Fei, and T. Zhang, *Sens. Actuators B* 202, 272 (2014).
14. J.E. Koo, S.T. Lee, and J.H. Chang, *J. Nanosci. Nanotechnol.* 15, 669 (2015).
15. H. Ko, S. Park, S. Park, and C. Lee, *J. Nanosci. Nanotechnol.* 15, 5295 (2015).
16. T. Xiang, Z. Lin, and Y. Qu, *J. Nanosci. Nanotechnol.* 15, 4493 (2015).
17. R.J. Oweis, B.A. Albiss, M.I. Al-Widyan, and M.A. Al-Akhras, *J. Electron. Mater.* 43, 3222 (2014).
18. D. Zhang, J. Tong, B. Xia, and Q. Xue, *Sens. Actuators B* 203, 263 (2014).
19. K.R. Nemade and S.A. Waghuley, *J. Electron. Mater.* 42, 2857 (2013).
20. D.Z. Zhang, A.M. Liu, H.Y. Chang, and B.K. Xia, *RSC Adv.* 5, 3016 (2015).
21. X. Wang, B.L Li, D.P Liu, and H.M Xiong, *Sci China Chem.* 57, 122 (2014).
22. S.S. Wei, L.Y. Wang, M.L. Yu, X.Y. Xu, and X.H. Chen, *J. Bionanosci.* 8, 298 (2014).
23. S. Deng, V. Tjoa, H.M. Fan, H.R. Tan, D.C. Sayle, M. Olivo, S. Mhaisalkar, J. Wei, and C.H. Sow, *J. Am. Chem. Soc.* 134, 4905 (2012).
24. S. Srivastava, K. Jain, V.N. Singh, S. Singh, N. Vijayan, N. Dilawar, G. Gupta, and T.D. Senguttuvan, *Nanotechnology* 23, 205501 (2012).
25. Z.X. Jiang, J. Li, H. Aslan, Q. Li, Y. Li, M.L. Chen, Y.D. Huang, J.P. Froning, M. Otyepka, R. Zbořil, F. Besenbacherb, and M.D. Dong, *J. Mater. Chem. A* 19, 6714 (2014).
26. S.M. Liang, J.W. Zhu, C. Wang, S.T. Yu, H.P. Bi, X.H. Liu, and X. Wang, *Appl. Surf. Sci.* 292, 278 (2014).

27. G. Neri, S.G. Leonardi, M. Latino, N. Donato, S. Baek, D.E. Conte, P.A. Russo, and N. Pinna, *Sens. Actuators B* 179, 61 (2013).
28. W.J. Yuan, A.R. Liu, L. Huang, C. Li, and G.Q. Shi, *Adv. Mater.* 25, 766 (2013).
29. Y.H. Chang, Y.F. Yao, B. Wang, H. Luo, T.Y. Li, and L.J. Zhi, *J. Mater. Sci. Technol.* 29, 157 (2013).
30. G. Neria, S.G. Leonardia, M. Latinob, N. Donato, S. Baek, D.E. Conte, P.A. Russo, and N. Pinna, *Sens. Actuators B* 179, 61 (2013).
31. H.J. Kim and J.H. Lee, *Sens. Actuators B* 192, 607 (2014).
32. S. Mao, S. Cui, G. Lu, K. Yu, Z. Wen, and J. Chen, *J. Mater. Chem.* 22, 11009 (2012).
33. M. Tonezzer and R.G. Lacerda, *Sens. Actuators B* 150, 517 (2010).
34. P.A. Russo, N. Donato, S.G. Leonardi, S. Baek, D.E. Conte, G. Neri, and N. Pinna, *Angew. Chem. Int. Ed.* 51, 11053 (2012).
35. Y.B. Tang, C.S. Lee, J. Xu, Z.T. Liu, Z.H. Chen, Z.B. He, Y.L. Cao, G.D. Yuan, H.S. Song, L.M. Chen, L.B. Luo, H.M. Cheng, W.J. Zhang, I. Bello, and S.T. Lee, *ACS Nano* 4, 3482 (2010).
36. S.Z. Deng, V. Tjoa, H.M. Fan, H.R. Tan, D.C. Sayle, M. Olivo, S. Mhaisalkar, J. Wei, and C.H. Sow, *J. Am. Chem. Soc.* 134, 4905 (2012).